# Size-selective deposition of particles combining liquid and particulate dielectrophoresis

M. R. King[a] and O. A. Lomakin
*Department of Biomedical Engineering, University of Rochester, Rochester, New York 14627*

R. Ahmed and T. B. Jones
*Department of Electrical and Computer Engineering, University of Rochester, Rochester, New York 14627*

(Received 20 October 2004; accepted 30 November 2004; published online 8 February 2005)

Rapid, size-based, deposition of particles from liquid suspension has been demonstrated using the nonuniform electric field created by coplanar microelectrode strips patterned on an insulating substrate. The scheme uses the dielectrophoretic force both to distribute aqueous liquid containing particles and, simultaneously, to separate the particles. Tests conducted with solutions containing equal volume fractions of 0.53 and 0.93 $\mu$m polystyrene beads, tagged with different fluorescent dyes, reveal size-based separation within nanoliter droplets formed along the structure after voltage removal. The relative volume ratio of the two sizes varies smoothly from 1:1 to ~3:1 (favoring the smaller particles) along the electrodes. Using the Clausius–Mossotti factor $\underline{K}$ as the only adjustable parameter, the experimental data correlate to a numerical simulation of the process at $\mathrm{Re}[\underline{K}] \approx 0.5$, a value consistent with expectation for polystyrene beads at ~100 kHz in aqueous suspension. © *2005 American Institute of Physics*. [DOI: 10.1063/1.1852694]

## I. INTRODUCTION

Many schemes exploiting electrostatic forces in practical implementations of the laboratory-on-a-chip are now under investigation.[1] Ranging widely in form, the concepts fit loosely into two categories: (i) microfluidic plumbing systems, intended for movement, manipulation, and dispensing of liquid samples, and (ii) particle control schemes, for collecting, separating, positioning, and characterizing suspended biological cells, organelles, or macromolecules. There are clear functional advantages when fluidic and particulate control can be combined in one microsystem. We describe here a very simple electrode structure that dispenses nanoliter aqueous droplets starting from an initial microliter-sized sample and, simultaneously, performs size-based separation of submicron particles suspended in the liquid. The transient actuation and separation processes take place within ~100 ms.

Nonuniform ac electric fields imposed by planar electrodes patterned on an insulating substrate and coated with a thin, dielectric layer can be used to manipulate, transport, dispense, and mix small samples of aqueous liquids.[2,3] This scheme, dielectrophoretic (DEP) liquid actuation, exploits the ponderomotive force exerted on all dielectric media by a nonuniform electric field. It is closely related to electrowetting on dielectric-coated electrodes (known as EWOD).[4–7] In fact, EWOD and DEP liquid actuation are, respectively, the low- and high-frequency limits of the electromechanical response of aqueous liquid masses to a nonuniform electric field.[8,9] For the present application, high frequency is requisite so that the electric field can permeate the liquid and exert the desired DEP force on the suspended particles. At the lower frequencies used for electrowetting, this force cannot be exploited because the electric field is blocked from the interior of the liquid if the electrodes are dielectric coated.[10]

The scheme described in this paper is similar to field flow fractionation (FFF). In FFF, particles dispersed in a liquid flow are subjected to a controllable transverse force field. Typically, this force field distributes the particles at varying heights above a surface, thereby placing them on faster or slower-moving streamlines in the flow field.[11] Each particle seeks its equilibrium, dependent on its individual properties, at the height where the applied force balances sedimentation, and then is swept along at the velocity of the fluid corresponding to that height. Thus, an initially homogeneous mixture will fractionate; particles carried along by the flow at different rates will emerge at the outlet at different times.

DEP-based FFF typically uses an upward-directed (negative) DEP force effectively to levitate the particles.[12] It has been used to separate latex microspheres[13] and blood cells.[14] Our process differs from these continuous flow schemes in that it is transient and nonequilibrium. Particles suspended in the parent drop are drawn into the finger and swept rapidly along by the liquid, while at the same time being attracted toward the strip electrodes by a downward-directed, *positive* DEP force. Rather than remaining suspended at a constant equilibrium height as in conventional FFF, particles in DEP microactuation follow essentially curved trajectories as depicted in Fig. 1(c). Gravity plays no role; the time for a 1 $\mu$m latex bead to settle a distance of 30 $\mu$m, a distance comparable to the height of a liquid finger, is $\sim 10^3$ s, while the transient finger motion requires only $\sim 10^{-1}$ s.

## II. EXPERIMENT

Figure 1 shows the planar electrode structure used in the experiments. The parallel electrode strips, patterned in 2 kÅ

[a]Electronic mail: mike_king@urmc.rochester.edu

 

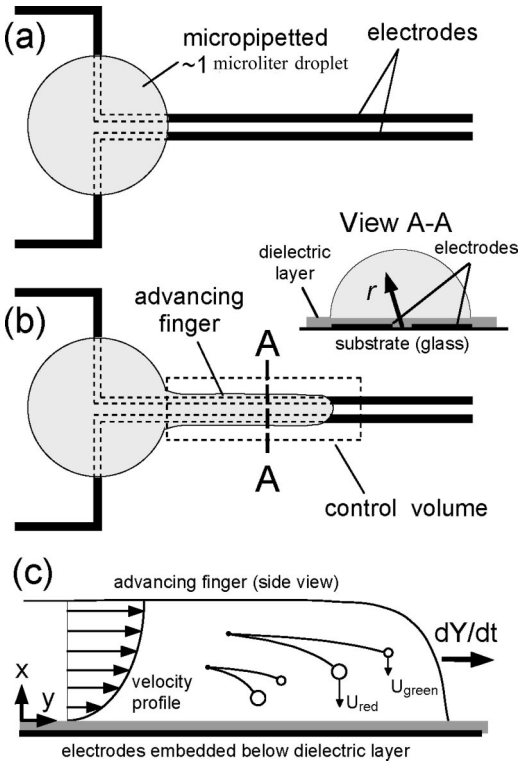


FIG. 1. Parallel, coplanar electrodes used to actuate liquid with sessile droplet dispensed from a micropipette. (a) Top view before application of voltage. (b) After voltage is applied, a finger of approximately semicircular cross section emerges and moves rapidly along the electrodes, stopping when it reaches the end. (c) Side view of advancing finger depicting velocity profile and field flow fractionation mechanism resulting from downward-directed, size-dependent DEP force on the suspended particles. Larger beads drift more rapidly toward the surface and on average travel along slower-moving streamlines. The smaller particles are convected further along the structure, resulting in size-based separation.

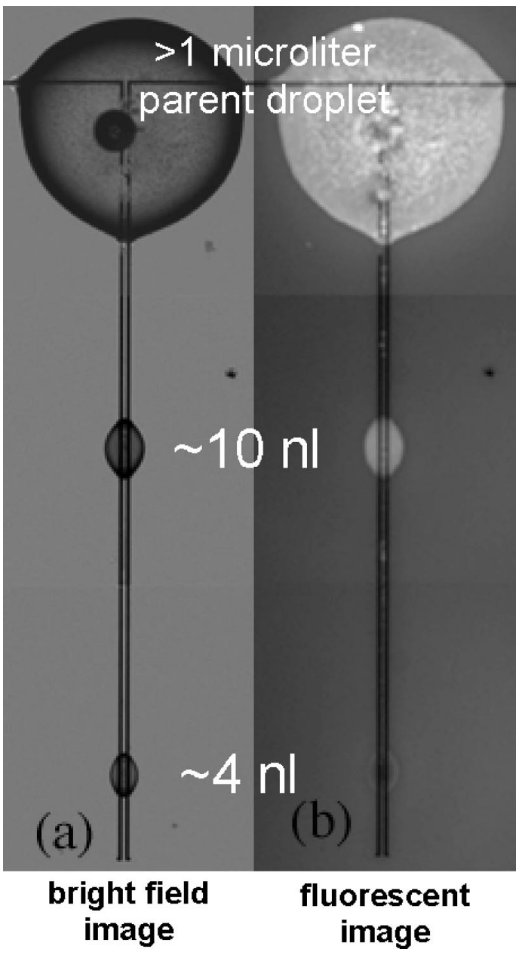


FIG. 2. Bright field (a) and fluorescent (b) images of DEP droplet dispenser, showing strong spatially dependent transport of suspended, fluorescent-tagged 0.53 $\mu$m particles from the parent droplet (top of image) to two droplets formed along electrode structure (below). The initial particle volume fraction was 0.06%. Relative fluorescent intensities indicate that density of particles in second droplet is much lower than in the first droplet. Electrodes are coplanar strips patterned in 2 kÅ Al strips, 20 $\mu$m wide, spaced at 20 $\mu$m, 3 mm long, and coated with 2 $\mu$m of SU-8™ and ~0.5 $\mu$m of photoresist. Voltage (250 V rms @ 100 kHz) applied for several hundred milliseconds, long enough for the finger to reach the end of the electrodes. Droplets formed by capillary instability in <10 ms upon removal of voltage.

thick Al evaporatively deposited on borosilicate glass substrates, were of width $w=20$ $\mu$m, separation $g=20$ $\mu$m, and length=6 mm. These structures were spin-coated, first with ~2 $\mu$m of SU-8™, an epoxy-based, dielectric material, and then with ~0.5 $\mu$m of photoresist (Shipley 1805) to control wetting. To facilitate quantitative investigation of the separation effect, we suspended fluorescent-labeled, polystyrene microspheres (0.53 and 0.93 $\mu$m diameter, 0.06% by volume; Bangs Labs, Fishers, IN) in deionized water, adding nonionic surfactant to prevent particle aggregation (Tween 20, 0.1%–0.5% by volume). Prior to each experiment, the–COOH surface groups of the microspheres were covalently coupled to ethanolamine using a single step reaction, rendering the beads uncharged and hydrophilic.[15] The ethanol layer on the particle surface acts to reduce the hydrophobic nature of the polystyrene beads, although not completely as discussed below. In all experiments, the substrates were mounted horizontally and covered by a few millimeters of oil—typically, embryo-safe mineral oil (Sigma)—to minimize wetting stiction and hysteresis. The oil provided the added benefit of eliminating evaporation.

Initial experiments were performed with monodisperse suspensions of 0.53 $\mu$m particles. To prepare for each experiment, a ~1 $\mu l$ parent droplet of the test liquid was dispensed from a micropipette at one end of the structure (top of Fig. 2). Then, 250 V rms at 100 kHz was applied for less than 1 s, causing a finger to protrude from the sessile droplet and to move rapidly along the electrodes to the opposite end as depicted in Fig. 1(b). When voltage was removed, capillary instability very rapidly broke up the finger into droplets distributed along the electrodes. The number of daughter drops produced by rupture of the finger is related to the interfacial tension.[3] Directly following each experiment, the substrates were imaged on an inverted, fluorescence microscope (Olympus IX81; Olympus America, Inc., Melville, NY) equipped with a high-resolution, cooled charge-coupled device (CCD) camera (Sensicam QE; Cooke Corp., Auburn Hills, MI). The bright field image of Fig. 2(a) shows that two droplets formed having volumes ~10 and ~4 nl, respectively. Figure 2(b) a fluorescent image of the same scene, reveals that the ~4 nl droplet, further from the parent droplet, has a bead concentration manifestly lower than the closer, ~10 nl droplet. Some plating out on the electrodes

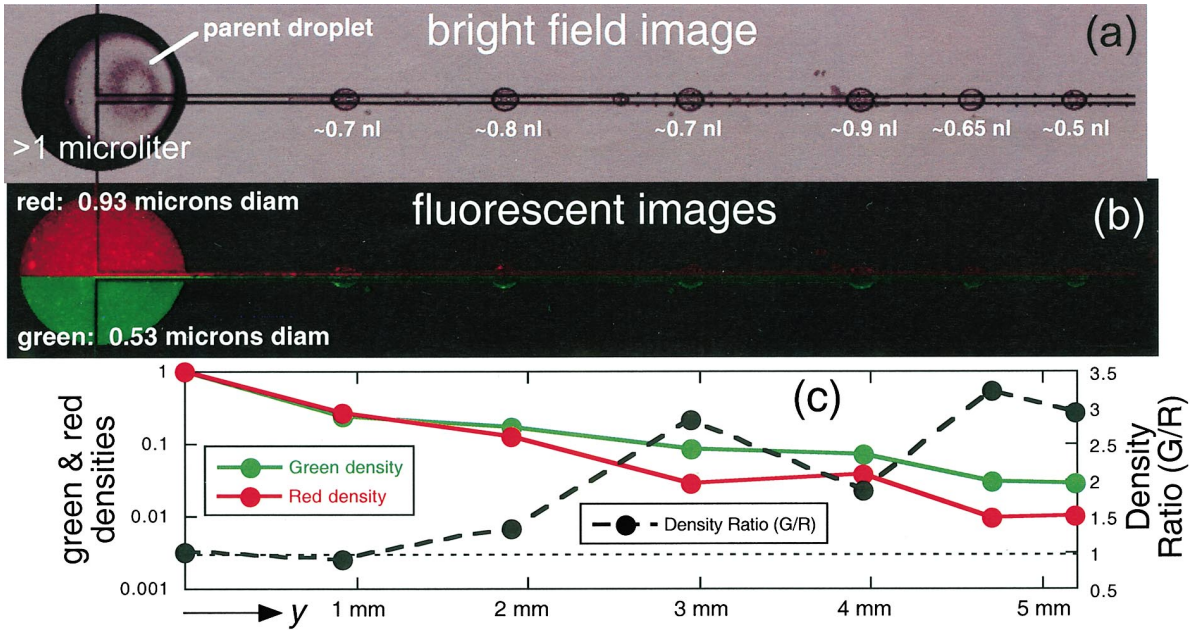


FIG. 3. (Color) Composite bright field (a) and fluorescent (b) images of DEP droplet dispenser show size-based deposition of fluorescent-tagged particles within six daughter droplets formed along electrode structure (to right of parent droplet). Initial 0.53 $\mu$m (green) and 0.93 $\mu$m (red) particle volume fractions in parent droplet are identical: 0.03%. Pseudocolor image is a spliced composite of green and red fluorescent micrographs of the same scene, showing the differences in the particle distributions along the electrodes. (c) Logarithmic plot of average intensity quantifies the particle separation. Coplanar electrodes are identical to Fig. 2, except 6 mm in length. Voltage is 275 V rms@ 100 kHz applied for a few hundred milliseconds.

between the droplets is evident, indicating that the particles retain some hydrophobic property by adhering to the electrodes on contact with them due to nonspecific adhesion.

This indication of particle separation along the length of the structure encouraged us to conduct additional experiments using suspensions containing equal parts by volume (0.03% for each) of 0.53 and 0.93 $\mu$m beads to determine if size-based separation could be achieved. To facilitate simultaneous measurement of the two subpopulations, the smaller beads were labeled with Dragon Green dye (excitation/emission=480/520 nm; Bangs Labs, Fishers, IN) and the larger beads with Flash Red dye (660/690 nm; Bangs Labs). The result of one experiment is shown in Fig. 3. The bright field image in Fig. 3(a) shows six fairly uniform droplets (plus one small satellite, which was ignored). Adjacent to this image is another image (b) of the same scene, created by splicing together opposite halves of the red and green fluorescent photomicrographs. From the split image, it is readily apparent that the green (smaller) particles were transported further along the structure by DEP-actuated flow. This visual impression is borne out by optical density data plotted in Fig. 3(c), directly beneath the fluorescent composite image. These data, indicating average green and red densities within each droplet, were obtained from integration of the fluorescent intensities and division by the image areas of each droplet. The plotted color intensity values were normalized with respect to their corresponding average intensities of the parent droplet, and the local background intensity measured between daughter droplets was subtracted out. Because the particle suspensions are very dilute ($\ll$1%), it is justified to assume that the integrated fluorescence intensities are linearly proportional to the total number of beads contained within each droplet, and thus provide an accurate measure of local particle concentrations. Moving away from the parent droplet, the absolute densities of both size cuts drop almost monotonically, with the density of the larger (red) particles decreasing more rapidly. The green/red density ratio, 1:1 in the test solution, has reached $\sim$3:1 for the sixth droplet, situated $\sim$5 mm from the edge of the parent droplet.

## III. MODEL

To investigate the mechanisms at work in the transient DEP particle separation scheme, we developed a simple model for the process and then used a simulation methodology with a single adjustable parameter related to the particle polarizability for comparison to the concentration data plotted in Fig. 3(c).

### A. Dielectrophoretic force on particles

Particles swept along in the $z$ direction by the rapidly moving finger experience a transverse (downward-directed) DEP force induced by the nonuniform electric field created by the parallel electrodes. This force, acting primarily in the radial $r$ direction as depicted in the cross section of Fig. 1(b), may be expressed in standard form as[16]

$$F_{\mathrm{DEP},r} = 2\pi\varepsilon_m R^3 \,\mathrm{Re}[\underline{K}]\partial E^2/\partial r. \tag{1}$$

In Eq. (1), $R$ is particle radius, $\varepsilon_m$ is permittivity of the suspension medium, $E(x)$ is magnitude of the transverse electric field, and $\underline{K}$ is the complex, frequency-dependent Clausius–Mossotti factor.

$$\underline{K}(\omega) = \frac{\underline{\varepsilon}_p - \underline{\varepsilon}_m}{\underline{\varepsilon}_p + 2\underline{\varepsilon}_m}, \tag{2}$$

where $\underline{\varepsilon}_p$ is the complex permittivity of the particle, $\underline{\varepsilon}_m = \varepsilon_m + 1/j\omega\sigma_m$ is the complex permittivity of the liquid medium, $\omega$ is the ac electric field frequency in rad/s, and $\sigma_m$ is the electrical conductivity. The sign of $\mathrm{Re}[\underline{K}]$ determines the direction of the DEP force: for $\mathrm{Re}[\underline{K}]>0$ (positive DEP), particles are attracted toward the gap between the electrodes where the electric field is strongest while for $\mathrm{Re}[\underline{K}]<0$ (negative DEP), particles are repelled.

While values for $\varepsilon_m$ and $\sigma_m$ are generally known, or readily measurable, $\underline{\varepsilon}_p$ is more difficult to characterize for submicron polystyrene beads in aqueous suspension due to imperfect knowledge of interfacial conditions.[17,18] One may exploit the condition $-0.5 \geqslant \mathrm{Re}[\underline{K}] \geqslant 1.0$ to establish firm upper and lower limits for the DEP force magnitude. The approach in this paper is to treat $\mathrm{Re}[\underline{K}]$ as the adjustable parameter in simulations based on the model, using the experimental data to establish an estimate for this quantity. We then compare this estimate to values reported in prior investigations with comparable particles.

### B. Nonuniform electric field model

Because of the high dielectric constant of the water, $\kappa_m \sim 80$, interior electric field lines near the curved upper boundary of the liquid finger are constrained to be circular arcs. Thus, the nonuniform field is essentially azimuthal and its spatial nonuniformity may be approximated by an inverse dependence on the radial distance $r$ measured from an imaginary axis running along the surface midway between and parallel to the electrodes.

$$E_\varphi(r) \approx V/\pi r, \tag{3}$$

where $V_{\mathrm{finger}}$ is the voltage drop that occurs within the finger, which is less than the applied voltage $V$ because of capacitive voltage division.

$$V_{\mathrm{finger}} \approx \frac{C_d}{2C_m + C_d} V, \tag{4}$$

where $C_d = \kappa_d \varepsilon_0 w/d$, $C_{\mathrm{air}} = \varepsilon_0 K(1-\zeta)/2K(\zeta)$, and $C_m = \kappa_m C_{\mathrm{air}}$ are, respectively, the per unit length capacitances of the dielectric layer, the coplanar electrode structure in air, and the same structure with the water finger present.[2] $K$ is the complete elliptic integral with argument $\zeta \equiv g/2(w+g/2)$. Combining Eqs. (3) and (1) gives the DEP force on the particles.

$$F_{\mathrm{DEP},r} = -\frac{4\varepsilon_m R^3 \,\mathrm{Re}[\underline{K}]}{\pi r^3} V_{\mathrm{finger}}^2. \tag{5}$$

This force exhibits rather strong inverse dependence on $r$. For particles close to the axis, $0<r<g/2$, Eq. (3) suffers from inaccuracy; however, the separation process is dominated by the behavior in regions where particles move slowest, that is, where the field gradient is weakest. Thus, we anticipate that the inaccuracy of Eq. (3) close to the axis will have limited overall influence on the predictions of the model.

### C. Radial motion of particles

As the liquid sweeps particles along the structure in the $y$ direction, the DEP force simultaneously attracts them toward the gap between the electrodes. Opposing this force is the Stokes drag.

$$F_{\mathrm{drag},r} = -6\pi\mu_m R U_r, \tag{6}$$

where $\mu_m$ is the liquid viscosity and $U_r$ is the radial component of particle velocity. As particles drift closer to the electrodes, they encounter a steadily stronger DEP force and, simultaneously, slower moving liquid. Equating Eqs. (5) and (6) reveals a strongly size-dependent radial drift,

$$U_r = -\frac{2\varepsilon_m R^2 \,\mathrm{Re}[\underline{K}]}{3\pi^2 \mu_m r^3}\left(\frac{C_d}{2C_m + C_d} V\right)^2. \tag{7}$$

Because $U_r$, the Stokes velocity, is proportional to $R^2$, on average the larger beads are drawn preferentially toward the electrode surface, where the liquid is slower moving. The smaller particles, remaining more evenly distributed throughout the cross section of the finger, travel further on average, and collect preferentially in daughter droplets formed further from the parent. This nonequilibrium FFF mechanism is responsible for the size-based separation evident in Fig. 3.

### D. Dynamics of the finger

The simulation requires a model for the transient dynamics of the finger. The methods of lumped parameter electromechanics based on variable capacitance[19] provide an attractive way to predict the net force of electrical origin on the liquid mass. We write the momentum conservation equation for a control volume containing the entire lengthening finger as shown in Fig. 1(b).

$$\frac{d}{dt}\left(\rho_m A_x Y \frac{dY}{dt}\right) = f^e + f_{\mathrm{drag}} + f_{st}, \tag{8}$$

where $\rho_m$ is the liquid density, $A_x \approx (\pi/2)(w+g/2)^2$ is the semicircular cross section of the finger, and $Y(t)$ is the time-dependent finger length. The electromechanical force driving the finger is

$$f^e = \frac{(\kappa_w - 1) C_d C_{\mathrm{air}} V^2}{2(C_d + 2C_m)}, \tag{9}$$

where $\kappa_m$ is the dielectric constant of the water and $V$ is the rms voltage.

The drag force in Eq. (8) may be expressed as

$$f_{\mathrm{drag}} = -P_{\mathrm{finger}} Y(t) \tau_{\mathrm{drag}}, \tag{10}$$

where $P_{\mathrm{finger}}$ is the total perimeter of the finger, $\tau_{\mathrm{drag}} = \mu_m \partial U_y/\partial x$ is the shear stress, and $\mu_m$ is dynamic viscosity. The surface tension is approximated by

$$f_{st} = -\gamma P_{\mathrm{finger}}, \tag{11}$$

where $\gamma$ is the interfacial tension.

On the time scale of interest for DEP actuation, that is, $0.01\ \mathrm{s} < t < 1.0\ \mathrm{s}$, momentum is safely neglected in Eq. (8) so that the dynamic equation for the finger becomes

$$P_{\text{finger}}Y(t)\tau_{\text{drag}} \approx \frac{(\kappa_w - 1)C_d C_{\text{air}} V^2}{2(C_d + 2C_m)} - \gamma P_{\text{finger}}, \tag{12}$$

where $\tau_{\text{drag}} \propto dY/dt$ must be determined from the velocity profile within the liquid finger.

### E. Velocity profile

Consider the cross section of the liquid finger as shown in Fig. 1(b), view *A*-*A*. The velocity profile for a half cylinder of fluid set in motion by a body force can be obtained by a conformal mapping transformation of the spatial coordinates. First, the transverse coordinates $(x,z)$ are normalized by the height of the liquid finger $H=w+g/2$, i.e., $x'=x/H$ and, $z'=z/H$. A circle defines the upper fluid interface: $(x')^2+(z')^2=H^2$. Then, the dimensionless coordinates are stretched by the hyperbolic sine and cosine so that the upper interface is defined by

$$\frac{(x')^2}{\sinh(1)} + \frac{(z')^2}{\cosh(1)} = 1. \tag{13}$$

The result is a transformed coordinate system that admits a simple solution for the velocity profile. In the new coordinate system $(u,v)$, related to the original coordinates by $v+ju=\sin(y+jx)$ with $j=\sqrt{-1}$, the original semicircular cross section becomes a rectangular domain $v \in [-\pi/2, +\pi/2]$, $u \in [0,1]$. The upper surface of the rectangular domain ($u=1$) corresponds to the curved upper free surface of the finger, while the sides and bottom map to its boundary on the substrate. The solution for a pressure or body-force driven flow of liquid through a rectangular conduit with a free (zero-shear) upper surface and no-slip conditions on the sides and bottom is

$$U(v,u) = U_{\max} u^2 (v - \pi/2)^2. \tag{14}$$

The main features of the unidirectional velocity profile are that it reaches its maximum at the highest point of the finger and goes to zero on the substrate, $x=0$.

The desired velocity profile and the shear stress $\tau_{\text{drag}}$ in $(x,z)$ coordinates are obtained through the coordinate transformation given above. The area-averaged fluid velocity was numerically determined to be $U_{\text{avg}}=dY/dt=0.2202U_{\max}$. From scaling arguments, the average wall shear stress $\tau_{\text{drag}}$ is

$$\tau_{\text{drag}} = \frac{2\mu}{w + g/2}\frac{dY/dt}{c}, \tag{15}$$

where $c$ is an $O(1)$ constant that depends on the details of the flow. Numerical integration of the velocity gradient at the wall using the detailed solution described above yields $c=0.507$.

When Eq. (15) is used in Eq. (12), the resulting differential equation can be solved analytically,

$$Y(t) = A\sqrt{t}, \quad \text{where } A = \sqrt{\frac{0.507(f^e + f_{st})(w + g/2)}{\mu(P_f + 2w + g)}}. \tag{16}$$

The $\sqrt{t}$ time dependence of the finger length is identical to certain thermocapillary driven flows.[20] Note the scaling of finger growth time with respect to electrode structure length $L$,

$$t_f = L^2/A^2. \tag{17}$$

### F. Deficiencies of the model

The model described above neglects the effect of Brownian particle diffusion, which for a 1 $\mu$m particle in water at 300 K is characterized by a diffusivity of 0.4 $\mu m^2/s$. Thus, this effect is expected to be too slow to influence the DEP-driven dynamics. It is possible that diffusion could have influenced our data nevertheless, since microscopic imaging was performed up to 2 h after experiments had been performed. However, because most of the particles have already been deposited or are contained within discrete droplets, we do not believe this to be important. Another limitation of the simulation is that the two-dimensional flow model ignores the 3D nature of the flow at the leading edge of the flowing finger. For the flow in this region to have a significant influence on deposition, it would be necessary for a significant fraction of the suspended particles to be drawn forward and then downward toward the substrate. At present, we have no means to estimate the possible significance of such an effect.

## IV. NUMERICAL SIMULATIONS

The system of equations describing finger elongation and simultaneous particle motion was integrated numerically as an initial value problem with particles randomly distributed throughout the cross section and introduced into the flow at the inlet to the finger. The location of each particle, governed by Eq. (7), was tracked as a function of time. Steadily increasing time steps, corresponding to fixed discrete displacements of the leading edge of the finger were implemented for computational efficiency:

$$dt_i = \left\lfloor \left(\frac{L_i}{A}\right)^2 - \left(\frac{L_{i-1}}{A}\right)^2 \right\rfloor, \tag{18}$$

with a fixed spatial step size: $dL=L_i-L_{i-1}$. This variable time step approach facilitates fixing the number of beads introduced at each time step to be constant, corresponding to the requirement of uniform bead concentration in the parent droplet. The probability density of particles at the inlet to the finger must be correctly weighted with the fluid flux distribution in the axial ($y$) direction at the inlet [proportional to $U(x,z;t)$ given above]. We impose this constraint by generating a group of three random numbers $(x',y',z')$ uniformly distributed between 0 and 1. If $y' < U(x',z')$ where $U$ is the dimensionless fluid velocity, then $x'$ and $z'$ are used as the initial coordinates of the entering particle in the finger cross section. Groups of random numbers are generated until this test is satisfied for each new particle placement. Such a weighting properly distributes particles at the inlet ($y=0$) in accord with the assumption of a uniform distribution of particles within the feed droplet. In all numerical results shown, 1000 time steps and 1000 particles were used.

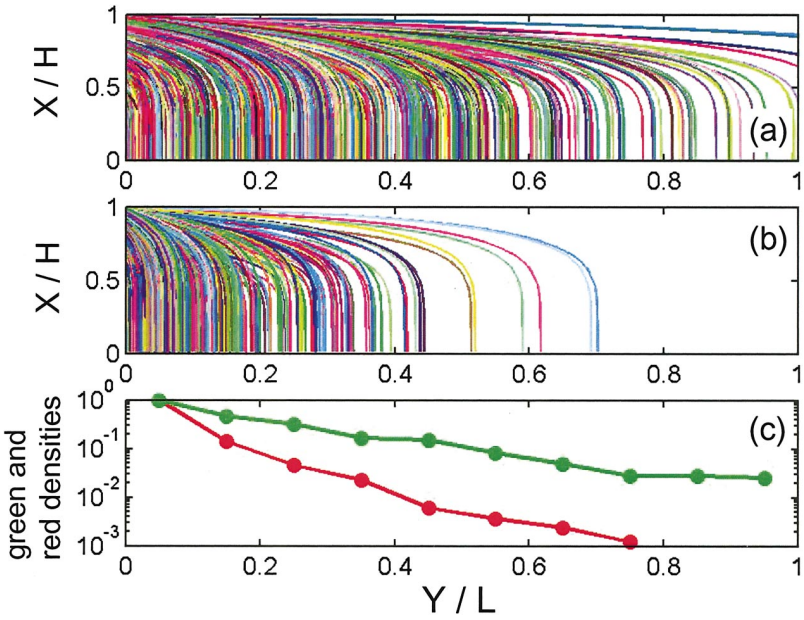


FIG. 4. (Color) Results of 3D Monte Carlo simulation of DEP particle flow of a bidisperse mixture for the experimental conditions of Fig. 3 using $\mathrm{Re}[\underline{K}]=0.5$. (a) Side view of sample trajectories for smaller particles (0.5 $\mu$m dia). (b) Side view of trajectories for larger particles (1.0 $\mu$m dia). (c) Normalized particle densities for the smaller (green) and larger (red) particles.

### Parameter fitting for $\underline{K}(\omega)$

Polystyrene beads in aqueous solutions exhibit strong, frequency-dependent behavior in the form of a prominent relaxation process. At low frequencies, $\mathrm{Re}[\underline{K}]\sim 1$, while at high frequencies, $\mathrm{Re}[\underline{K}]\approx -0.50$.[21] The key to estimating $\mathrm{Re}[\underline{K}]$ is to have reliable information about the crossover frequency that divides these regions. For polystyrene beads in the 0.5–1.0 $\mu$m range suspended in aqueous media of electrical conductivity $\sigma_m \leqslant 2\times 10^{-3}$ S/m, the crossover frequency typically exceeds 1 MHz.[12,17,22] Our medium conductivity probably did not exceed $\sim 10^{-3}$ S/m so we may assume that our experiments, all performed using 100 kHz ac, were far below the crossover. Thus, we would expect that $0.8 \leqslant \mathrm{Re}[\underline{K}] \leqslant 1.0$.

A range of values for the Clausius–Mossotti factor was used in the simulation in an effort to reproduce the experimental data plotted in Fig. 3. Figure 4 summarizes results from a representative simulation using $\mathrm{Re}[\underline{K}]=0.5$ and with all other parameters set to the experimental conditions. Figures 4(a) and 4(b) show side views of sample trajectories for the smaller (0.5 $\mu$m diameter) and larger (1.0 $\mu$m) beads, respectively. Note that none of the larger particles are convected beyond $y\approx 0.7$ L. Fig. 4(c) displaying normalized bead densities for the smaller (green) and larger (red) particles, indicates that excellent beneficiation of the smaller particles is possible under these experimental conditions. The simulation results fit the data best at $\mathrm{Re}[\underline{K}]\sim 0.5$, which is consistent with expectations for polystyrene beads, given the uncertainties in the parameters and in the model.

Discrepancies between the predictions of the model and the experimental data may be attributed to several factors such as particle aggregation, secondary flow effects, and modeling inaccuracies. Principal problems with the model are the assumed form of the electric field in the finger, Eq. (3), and the capacitive divider ratio used to determine the voltage distribution in the water, Eq. (4). Finite element analysis of the time-varying field distribution in the finger would no doubt provide a more reliable estimate for the nonuniform $E$ field. However, this level of detail may not be that critical for exploiting variable frequency DEP particle separation. A far more effective and sensitive strategy might be to operate at a frequency centered on the crossover, thus exploiting the difference between positive and negative DEP to separate bio-particles based on medically relevant attributes that reflect in the DEP spectra. In such schemes, precise information about the nonuniform electric field distribution would not be essential.

## V. CONCLUSION

It has been demonstrated that the DEP effect can be harnessed to move and dispense small volumes of liquid containing suspensions of particles in the submicron range and that these particles can be simultaneously separated based on their size. The separation occurs because the downward-directed, positive DEP force imposed by the nonuniform electric field within the liquid attracts the larger particles more strongly, leaving the smaller particles to be swept further along in the shear flow of the finger. Using two-color fluorescence microscopy, the separation of two size cuts of polystyrene beads, viz, 0.53 and 0.93 $\mu$m diameter, is easily discerned. The process is rapid, usually requiring $\sim 10^2$ ms for a structure 6 mm in length. Further investigation is needed to determine the size range over which separation can be achieved and the efficiency of the process. In addition, we must develop better suspension-forming protocols to control particle agglomeration, which can interfere with the separation process.

We present a simple model for the separation scheme, and simulations performed with this model correlate best to the experimental data using $\mathrm{Re}[\underline{K}(\omega)]\sim 0.5$, which is slightly below the expected range of 0.8–1.0. Given the uncertainties of the parameters as well as the approximate nature of the model, this value provides reasonable confirmation of the model. Though not demonstrated here, the use of frequency as a control parameter for transient particle separation may

facilitate gradient deposition of particles within monodisperse populations based on medically important attributes.

One application envisioned for our scheme is *in situ* surface array sensitization on a substrate, that is, exploiting DEP liquid actuation to distribute functionalized particles (such as colloidal Au) that subsequently attach to droplet-forming electrode structures described elsewhere.[3] The flow generated deposition automatically creates a smooth particle concentration gradient of functionalized spots useful for gradient-sensitive chemical assays in the laboratory-on-a-chip.

## ACKNOWLEDGMENTS

The authors are grateful to H. Morgan (University of Southampton, UK) and M. P. Hughes (University of Surrey, UK) for generously sharing their knowledge of the DEP spectra of polymer beads. This work was supported by grants to T.B.J. from the National Institutes of Health, the Center for Future Health of the University of Rochester, the National Science Foundation, and the Infotonics Technology Center, Inc. (NASA Grant No. NAG3-2744).

[1]B. H. Weigl, R. L. Bardell, and C. R. Cabrera, Adv. Drug Delivery Rev. **55**, 349 (2003).
[2]T. B. Jones, M. Gunji, and M. Washizu, J. Appl. Phys. **89**, 1441 (2001).
[3]R. Ahmed, D. Hsu, C. Bailey, and T. B. Jones, Proceeding of the Microchannels and Minichannels Conference (ASME), Rochester, NY, 2003.
[4]B. Berge, C. R. Acad. Sci., Ser. II: Mec., Phys., Chim., Sci. Terre Univers **317**, 157 (1993).
[5]W. J. J. Welters and L. G. J. Fokkink, Langmuir **14**, 1535 (1998).
[6]M. G. Pollack, R. B. Fair, and A. D. Shenderov, Appl. Phys. Lett. **77**, 1725 (2000).
[7]J. Lee, H. Moon, J. Fowler, T. Schoellhammer, and C.-J. Kim, Sens. Actuators, A **A95**, 259 (2002).
[8]T. B. Jones, J. Fowler, Y.-S. Chang, and C.-J. Kim, Langmuir **19**, 7646 (2003).
[9]T. B. Jones, K.-L. Wang, and D.-J. Yao, Langmuir **20**, 2813 (2004).
[10]The electric field inside a perfect conductor is zero. In the case of a finite conductor such as water adjacent to dielectric-coated electrodes, the electric field distribution is frequency dependent. For low frequency, free charge collects at the water/dielectric interface, blocking the field from within the more conductive water and, in the dc limit, mimicking the behavior of a perfect conductor. On the other hand, at high frequency, the field alternates so rapidly that surface charge cannot accumulate, in which case an electric field can exist inside the water. See Ref. 2.
[11]J. C. Giddings, Science **260**, 1456 (1993).
[12]H. Morgan and N. G. Green, *AC Electrokinetics: Colloids and Nanoparticles* (Research Studies Press, Baldock, UK, 2003), Sec. 12.3.
[13]X. B. Wang, J. Vykoukal, F. F. Becker, and P. R. Gascoyne, Biophys. J. **74**, 2689 (1998).
[14]J. Yang, Y. Huang, X. B. Wang, F. F. Becker, and P. R. Gascoyne, Biophys. J. **78**, 2680 (2000).
[15]G. Quash, A. M. Roch, A. Niveleau, J. Grange, T. Keolouangkhot, and J. Huppert, Immunomethods **22**, 165 (1978).
[16]T. B. Jones, *Electromechanics of Particles* (Cambridge University Press, New York 1995).
[17]M. P. Hughes, *Nanoelectromechanics in Engineering and Biology* (CRC, Boca Raton FL, 2003).
[18]Y. Huang, X.-B. Wang, F. F. Becker, and P. R. C. Gascoyne, Biophys. J. **73**, 1118 (1997).
[19]H. H. Woodson and J. R. Melcher, *Electromechanical Dynamics* (Wiley, New York, 1968), Part I, Chap. 3.
[20]A. A. Darhuber, S. M. Troian, and W. W. Reisner, Phys. Rev. E **64**, 031603 (2001).
[21]Many DEP separation and collection processes take advantage of the particle size and liquid conductivity-dependent crossover frequency, where the DEP force goes through zero, changing from positive to negative. See Refs. 12 and 17 for more information.
[22]D. J. Bakewell and H. Morgan, Meas. Sci. Technol. **15**, 254 (2004).